JCTC Journal of Chemical Theory and Computation

ARTICLE

pubs.acs.org/JCTC

All-Electron Scalar Relativistic Basis Sets for the Actinides

Dimitrios A. Pantazis*,†,‡ and Frank Neese*,†,‡

†Lehrstuhl für Theoretische Chemie, Institut für Physikalische und Theoretische Chemie, Universität Bonn, Wegelerstrasse 12, D-53115 Bonn, Germany

‡Max-Planck-Institut für Bioanorganische Chemie, Stiftstrasse 34-36, 45470 Mülheim an der Ruhr, Germany

Supporting Information

ABSTRACT: Increasing interest in the computational modeling of actinide compounds creates the need for alternative choices when in comes to fine tuning the computational methodology in order to best fit the problem at hand. All-electron scalar relativistic density functional theory can be a useful approach for a variety of actinide systems and would benefit from atomic basis sets geared to that level of theory. In this paper we present segmented all-electron relativistically contracted (SARC) basis sets for the complete actinide series $_{89}$Ac−$_{103}$Lr, optimized for use with the popular Douglas−Kroll−Hess to the second order and zeroth-order regular approximation scalar relativistic Hamiltonians. The quality of the SARC basis sets is assessed in terms of their intrinsic incompleteness and contraction errors, with respect to total energies, orbital properties, and ionization energies. Calculations on diatomic Ac and Lr molecules confirm that the valence-space construction results in negligible basis set superposition errors. The performance of the basis sets is further evaluated for molecular geometries, vibrational frequencies, and bond dissociation energies in an illustrative study of uranium fluorides UF_n (n = 1−6).

1. INTRODUCTION

Research into the chemistry of actinide systems[1] witnesses a steady growth owing to its wide-ranging implications for environmental safety, power production and contamination recovery. The challenges of nuclear waste disposal and the management or reprocessing of spent nuclear fuel require, among others, the understanding of actinide behavior in aqueous systems and the development of chemical procedures that will allow the successful elemental separation of mixtures containing different actinide (and lanthanide) species. Advances in these fields naturally depend upon detailed and in-depth understanding of the chemical and physical properties of molecular actinide species. Laboratory study of actinide systems is often frustrated by problems arising from the intense radioactivity of most nuclides and the high toxicity and instability of the complexes as well as the obvious sourcing limitations. This situation as well as the necessity for a comprehensive understanding of electronic structure highlights the importance of theoretical approaches to actinide research, a field that attracts ever-increasing interest in recent years.[2−7]

Compared to experimental work, computational actinide chemistry is confronted with a different but not less daunting set of challenges. In contrast to the lanthanide 4f orbitals, the 5f orbitals of the actinides are less core-like, resulting in increased 5f orbital contribution to bonding and reactivity.[8−13] Moreover, the energetic proximity of 5f, 6p, 6d, and 7s orbitals leads to many close-lying energy levels and a large number of accessible oxidation states, at least for the early members of the series.[1] Coupled to this electronic complexity is the significant relativistic effects[14] that define the profile of actinides. Correlation and relativistic effects are both large and typically of the same magnitude,[15] demanding their simultaneous and theoretically adequate treatment. Faced with these challenges, computational studies of actinide species have so far employed with varying success a variety of methodologies from the arsenal of quantum chemistry, both in terms of approximate treatments of electron correlation and in terms of approximations to the Dirac Hamiltonian.[16]

With regard to the basis sets used in the description of the actinide elements, effective core potentials (ECPs)[17−21] that are adjusted to reproduce relativistic reference data have proven successful in enabling a whole range of applications. Owing to the significant reduction in cost and the convenient inclusion of relativistic effects, the use of ECPs is now an established practice for the prediction of several properties, especially for density functional theory (DFT)[22,23] studies of larger molecules. Inherent in this approximation, however, is the reliance on a delicate balance between the more complete empirical modeling of relativistic effects achieved through a larger ECP core and the better modeling of energetics and reactivity achieved through a larger valence space. Inevitably, this balance can be difficult to achieve in practice for all possible properties of interest.[3,15,24−27]

Most importantly, all-electron calculations become an absolute requirement when properties of the inner shells are being probed, as for example in electron paramagnetic resonance (EPR), Mössbauer, or X-ray spectroscopy. X-ray absorption spectroscopy (XAS) is a prominent example of particular importance in actinide chemistry and speciation with applications in the study of actinide compounds as a sensitive and element-specific probe of electronic structure.[28,29] The pre-edge and edge region (X-ray absorption near-edge spectroscopy, XANES) arises from core−electron excitations into the valence and unoccupied levels and can thus provide information about the oxidation state, the properties of the frontier orbitals, and the valence structure of

Received: December 22, 2010
Published: February 16, 2011

the actinide absorber.[30,31] Another straightforward example that clearly requires explicit consideration of all electrons is any kind of topological analysis of electron densities,[32−34] where the replacement of the core electrons by an effective potential may create topological inconsistencies and artifacts that extend into the bonding region.[35]

The rich variety of available all-electron basis sets for the top part of the periodic table contrasts with the more limited choices available for the bottom part, especially for the actinide elements, while most of the existing basis sets are designed for either wave function-based correlation methods or spin-including relativistic approaches.[36−42] In the present paper we are specifically targeting a "middle-ground" theoretical level: DFT coupled with one of the widely available scalar relativistic Hamiltonians, the Douglas−Kroll−Hess[43−47] (DKH2, to second order), or the zeroth-order regular approximation[48−50] (ZORA). An interesting alternative to these approaches has been implemented in the PRIRODA code,[51] based on a four-component one-electron scalar relativistic approximation to the full Dirac equation where all spin−orbit terms are neglected.[52] Generally contracted correlation-consistent basis sets developed by Laikov are used in this approach.[53] Two prominent examples of all-electron basis sets constructed specifically for scalar relativistic Hamiltonians are the Slater-type ZORA basis sets implemented in the Amsterdam density functional code[54,55] and the atomic natural orbital (ANO) basis sets of Roos et al.,[56] designed on the basis of CASPT2 calculations with the DKH Hamiltonian. The applicability of the Slater basis sets is unfortunately limited within software that can make efficient use of Slater-type functions. On the other hand, whereas the generally contracted atomic natural orbital (ANO) basis sets are a reliable choice for multiconfigurational correlated ab initio calculations on small systems, they are cumbersome for DFT applications on medium to large molecules. In that case a segmented contraction is preferred to reduce the computational cost associated with the generation of two-electron integrals in most general-purpose quantum chemistry codes. A no less significant consideration is that convergence of DFT-calculated quantities in terms of polarization space is achieved much faster than in ab initio correlated calculations,[22,57] therefore an extensive high angular momentum correlation set only adds to the cost of the calculation and not to the accuracy of the results. A recent confirmation of this can be found in the ZORA-DFT study of nuclear electric field gradient (EFG) tensors by Aquino et al.[58]

In light of the above, it is desirable to have a family of standardized, compact, and efficient actinide Gaussian basis sets that are best suited to the requirements of the DFT-DKH2 and DFT-ZORA levels of theory. Building upon the same approach that was used in the development of segmented all-electron relativistically contracted (SARC) basis sets for lanthanides[59] and third-row transition metals,[60,61] we propose a series of SARC basis sets to cover the actinide elements. Exponents of the Gaussian primitives are derived from simple rules and contraction coefficients are determined separately for the ZORA and DKH2 schemes, since these two approximations produce differing shapes for the core orbitals.[60] The quality of construction of the new basis sets is evaluated here for a range of atomic and molecular properties. All SARC basis sets are part of the freely available ORCA program package.[62]

2. RESULTS AND DISCUSSION

2.1. Construction of Basis Sets. As with the corresponding SARC basis sets for the third-row transition metals[60] and the lanthanides,[59] the starting point was the set of innermost radial expectation values per angular momentum, obtained from atomic ground-state restricted open-shell Hartree−Fock (ROHF) calculations. The ROHF calculations followed Zerner's spin-averaged (SA) formalism,[63,64] a variant of the configuration-averaged approach that averages over all states of a given spin for a given configuration. Exponents from the universal Gaussian basis set (UGBS) of de Castro and Jorge[65,66] have served well for constructing large reference basis sets in previous studies, allowing us to obtain benchmark results that approximate the basis set limit of the employed methods. In order to ensure saturation of the one-electron reference space, we used here an extended range of UGBS primitive Gaussians that goes significantly beyond the original definition for the actinides. In the following, "UGBS" will refer to this extended uncontracted (34s25p21d17f) form that yields 333 basis functions per actinide atom.

Table 1. Radial Expectation Values of Innermost Orbitals (in Bohr) Determined from Spin-Averaged ROHF Calculations

	$\langle r_s \rangle$	$\langle r_p \rangle$	$\langle r_d \rangle$	$\langle r_f \rangle$
Ac	0.016994	0.060121	0.146637	0.371265
Th	0.016804	0.059413	0.144672	0.363124
Pa	0.016618	0.058720	0.142757	0.355433
U	0.016436	0.058044	0.140893	0.348091
Np	0.016258	0.057382	0.139076	0.341087
Pu	0.016084	0.056735	0.137304	0.334403
Am	0.015914	0.056103	0.135578	0.327988
Cm	0.015747	0.055485	0.133894	0.321830
Bk	0.015583	0.054880	0.132251	0.315984
Cf	0.015423	0.054288	0.130647	0.310431
Es	0.015266	0.053709	0.129082	0.305040
Fm	0.015112	0.053142	0.127553	0.299853
Md	0.014962	0.052586	0.126060	0.294860
No	0.014814	0.052042	0.124602	0.289846
Lr	0.014669	0.051510	0.123177	0.285174

The actinide atomic configurations and corresponding states that were employed are the following: Ac (d^1s^2, ^{2}D), Th (d^2s^2, ^{3}F), Pa ($f^2d^1s^2$, ^{4}K), U ($f^3d^1s^2$, ^{5}L), Np ($f^4d^1s^2$, ^{6}L), Pu (f^6s^2, ^{7}F), Am (f^7s^2, ^{8}S), Cm ($f^7d^1s^2$, ^{9}D), Bk (f^9s^2, ^{6}H), Cf ($f^{10}s^2$, ^{5}I), Es ($f^{11}s^2$, ^{4}I), Fm ($f^{12}s^2$, ^{3}H), Md ($f^{13}s^2$, ^{2}F), No ($f^{14}s^2$, ^{1}S), and Lr ($f^{14}d^1s^2$, ^{2}D). As seen from the orbital occupations, electrons in 6d orbitals are lower in energy than those in 5f orbitals early in the series. The 5f orbitals begin to be occupied at protactinium, and the 6d orbitals are not occupied again in the second half of the series. This relates to the well-known distinction between the "transition-metal-like" early actinides and the "lanthanide-like" late actinides.

The individual steps of the procedure for the construction of basis sets have been described in detail previously,[59,60] so here we draw attention to the different parameter choices that were found to be more suitable for the actinides. Point nuclei are used throughout this work. Radial expectation values $\langle r_l \rangle$ for the first s, p, d, and f orbitals obtained from the reference SA-ROHF/UGBS calculations (Table 1) were used for deriving the exponents α_l of the tightest s, p, d, and f functions according to $\alpha_l = 2k_l f_l^2/\pi\langle r_l \rangle^2$, where f_l = 1, 4/3, 8/5, and 64/35 (l = s, p, d, f) and k_l is a scaling factor adjusted to 25 000, 2500, 500, and 250 for s, p, d and f functions, respectively. This leads to the generator exponents listed in Table 2. Extensive testing in atomic calculations showed

Table 2. Maximum Exponents per Angular Momentum (in Bohr^{-2}) Used for the Construction of the SARC Basis Sets

	α_s	α_p	α_d	α_f
Ac	55109808.74124	782789.90010	37896.83656	3860.78816
Th	56363088.88972	801557.42322	38933.29154	4035.84133
Pa	57631858.17253	820588.66007	39984.83121	4212.38926
U	58915269.20406	839813.66697	41049.82023	4391.96026
Np	60212393.78258	859302.83100	42129.44229	4574.18427
Pu	61522220.62253	879013.38137	43223.87650	4758.86803
Am	62843653.32611	898929.09050	44331.42040	4946.84248
Cm	64183659.71229	919065.41601	45453.55550	5137.96262
Bk	65541743.54208	939440.76053	46590.64590	5327.84571
Cf	66908672.67154	960041.30864	47740.96677	5522.22151
Es	68291966.01786	980851.97769	48905.61460	5719.13577
Fm	69690927.07217	1001894.08989	50085.12219	5918.71181
Md	71095290.12593	1023192.45899	51278.52058	6120.85750
No	72522948.25117	1044695.31751	52485.58789	6334.45665
Lr	73963782.78321	1066386.17254	53706.99426	6543.71139

that these exponents are sufficiently steep to capture the essential effects of the ZORA and DKH2 scalar relativistic Hamiltonians without introducing numerical instabilities that are often encountered when extremely tight functions are employed with a point-nucleus model.[41] It should be noted that the use of finite nuclei typically requires more and steeper functions to properly describe the inner core region than those employed in the present basis sets, and thus a different set of exponents would need to be generated for this model. Finite nuclear volume effects are known to affect properties that depend strongly on the inner core electronic structure, such as indirect nuclear NMR nuclear spin−spin couplings[67] or hyperfine coupling constants.[68] An evaluation of nuclear volume effects for the f-block elements will be performed separately, along with a determination of the necessary SARC basis set adaptations.

Subsequently, primitive Gaussian-type functions were obtained from the series $\alpha_l x^{-i}$ (i = 1, 2, ...), where the adjustable parameter x dictates the spacing and thus the overall number of the primitives. To strike a balance between the size of the final basis set, the quality of the atomic description, the efficiency of the observed convergence behavior, and the optimal values of x were determined to be 2.20, 2.40, 2.50, and 2.60 for l = s, p, d and f, respectively. Test calculations showed that it is adequate to terminate the series using cutoffs of 0.02 for s functions, 0.08 for p and d functions, and 0.2 for f functions.

The resulting uncontracted basis sets have the form (29s20p16d12f) comprising 253 primitives in total. In the last step the innermost 9s, 8p, 7d, and 6f primitives were contracted to create the final basis sets with a [21s13p10d7f] pattern and 159 functions. In terms of size this is at most half as that of uncontracted ANO basis sets[56] and thus is deemed more appropriate for routine all-electron DFT calculations. Contraction coefficients were optimized separately for the DKH2 and ZORA scalar relativistic Hamiltonians to better fit the differential effects produced by each approximation. Finally, scaling the average of the two most diffuse f exponents by 3.75 generated a set of optional single g polarization functions. In molecular calculations employing the DKH2 or ZORA Hamiltonians these actinide basis sets would be best combined with the respective SARC basis sets for the third-row transition metals[60] and the lanthanides[59] or the relativistically recontracted variants of the Karlsruhe basis sets[69]

Table 3. Estimated Incompleteness Errors (E_h) from Comparison of the UGBS and SARC Basis Sets, Obtained from Spin-Averaged ROHF Calculations with the DKH2 Hamiltonian

	UGBS (333 functions)	SARC (159 functions)	ΔE
Ac	−25678.01500	−25677.00385	1.011
Th	−26420.77386	−26419.69307	1.081
Pa	−27177.98097	−27176.83141	1.150
U	−27950.04069	−27948.81676	1.224
Np	−28737.17789	−28735.87599	1.302
Pu	−29539.63524	−29538.25221	1.383
Am	−30357.79074	−30356.32206	1.469
Cm	−31191.86262	−31190.30413	1.558
Bk	−32041.77325	−32040.12197	1.651
Cf	−32908.42477	−32906.67684	1.748
Es	−33791.95896	−33790.11137	1.848
Fm	−34692.72632	−34690.77658	1.950
Md	−35611.09371	−35609.03970	2.054
No	−36547.44572	−36545.28681	2.159
Lr	−37501.95189	−37499.68810	2.264

for lighter elements,[60] all of which are part of the ORCA basis set library.[62] Complete listings of the presently derived SARC basis sets in input format are provided in the Supporting Information.

2.2. Evaluation of Basis Sets. Given the stated goal of constructing reasonably small basis sets, the evaluation of the SARC basis sets for the actinides proposed in this paper must first address the errors in total energies resulting from the restricted number of basis functions and from contraction of the innermost primitive Gaussians. In Table 3 we compare SAHF-DKH2 total electronic energies obtained with the [21s13p10d7f] SARC basis sets to those obtained with the uncontracted UGBS, the latter assumed to be a good approximation to the basis set limit. The energy difference, which can be taken as a numerical estimate of the incompleteness error, rises as we traverse the actinide series from 1.01 E_h for actinium to 2.26 E_h for lawrencium. These values are quite satisfying considering the significant reduction in size from the UGBS to the SARC basis sets. In fact, these incompleteness errors are even smaller than those obtained for the corresponding lanthanide SARC basis sets, which ranged from 1.07 E_h for lanthanum up to 3.98 E_h for lutetium.[59]

Part of the incompleteness error results from the contraction of the SARC basis sets. To quantify the contraction error additional calculations were performed with the fully uncontracted (29s20p16d12f) SARC basis sets. The energy difference between contracted and uncontracted forms ranges from 0.042 E_h to 0.096 E_h, which again compares favorably with the contraction errors of the lanthanide basis sets, 0.033 E_h for lanthanum to 0.074 E_h for lutetium. Thus, the contraction error of the actinide SARC basis sets represents roughly a constant 4% of their total incompleteness error, suggesting that the proposed contraction pattern is a reasonable compromise between flexibility, size, and accuracy of the basis set.

As an additional evaluation metric, the energies and the radial expectation values for the orbitals of the valence region are found to either coincide or differ insignificantly between the UGBS and SARC basis sets. Specifically, the energies of occupied 6d and 7s orbitals are practically identical, while the energies of the 5f orbitals obtained by SARC tend to be slightly stabilized compared to the UGBS values, by 0.05 eV on average. As anticipated,

Table 4. SAHF-DKH2 Orbital Energies (E_h) and Radial Expectation Values (Bohr) for Plutonium: Comparison between UGBS and SARC Basis Sets

	UGBS		SARC			
	E	$\langle r \rangle$	E	$\langle r \rangle$	ΔE	$\Delta\langle r \rangle$
1s	−4488.462	0.012	−4488.374	0.012	0.087	0.000
2s	−854.015	0.054	−854.051	0.054	−0.036	0.000
2p	−711.675	0.051	−711.738	0.051	−0.063	0.000
3s	−220.340	0.142	−220.398	0.142	−0.058	0.000
3p	−180.303	0.146	−180.354	0.147	−0.051	0.000
3d	−143.568	0.135	−143.624	0.135	−0.056	0.000
4s	−58.500	0.309	−58.546	0.309	−0.046	0.000
4p	−45.153	0.331	−45.180	0.332	−0.027	0.000
4d	−31.074	0.345	−31.098	0.345	−0.024	0.000
4f	−16.615	0.340	−16.650	0.340	−0.036	0.000
5s	−13.572	0.645	−13.584	0.645	−0.012	0.000
5p	−9.283	0.721	−9.284	0.721	−0.002	0.000
5d	−4.448	0.848	−4.447	0.849	0.001	0.001
6s	−2.152	1.450	−2.155	1.449	−0.003	−0.001
6p	−1.035	1.784	−1.034	1.785	0.001	0.000
7s	−0.186	4.513	−0.186	4.509	0.000	−0.004
5f	−0.340	1.347	−0.341	1.348	−0.001	0.001

the maximum 5f energy difference between SARC and UGBS is observed for the heaviest actinide, lawrencium, at −0.13 eV. Larger deviations are observed for the shells with main quantum number less than five. Differences from UGBS orbital energies reach their maximum at the chemically inert 1s orbital, which is thus identified as a principal source of the incompleteness error in the SARC basis sets. As an illustrative example of the above, a detailed picture of the differences in predicted orbital energies and radial expectation values between UGBS and SARC is provided in Table 4 for the case of plutonium. In terms of practical use, it is encouraging that the radial expectation values practically coincide all the way down to the core region, since this implies that the decreased size of SARC compared to UGBS does not compromise the reproduction of scalar relativistic effects in the core region.

2.3. Ionization Energies. In contrast to the lanthanides, practically no experimental data exists for the ionization energies of the actinides beyond the first ionization energy (IE_1). From the point of view of quantum chemistry, the prediction of reliable actinide IEs is far from trivial, since it requires the simultaneous high-level treatment of electron correlation and relativity. It is not our intention here to offer a recipe for the accurate prediction of actinide ionization energies. Rather, our priority is to verify the balanced construction and contraction of the SARC basis sets, which can be inferred by the absence of bias and of systematic errors compared with the large UGBS reference.

For this purpose we have calculated the first four ionization energies of the actinides using the SAHF-DKH2 approach with both basis sets. The first electron is removed from the 6d orbital in Ac, Pa, U, Cm and Lr, and from the 7s orbital in the other elements. The second ionization results in f-only configurations for the cations U^{2+} to No^{2+}, with a single electron occupying the 7s orbital in Ac^{2+}, Th^{2+}, Pa^{2+}, and Lr^{2+}. Formation of the M^{3+} cations leads to a closed radon shell for Ac^{3+} and to 5f electronic configurations ranging from $5f^1$ (Th^{3+}) to $5f^{14}$ (Lr^{3+}). Finally, the fourth ionization involves removal of a 5f electron in all cases,

Table 5. Comparison of UGBS and SARC Basis Sets for the First Four Ionization Energies (eV) of the Actinides[a]

	SARC				UGBS			
	IE_1	IE_2	IE_3	IE_4	IE_1	IE_2	IE_3	IE_4
Ac	4.27	10.53	16.59	46.07	4.24	10.52	16.58	46.08
Th	4.59	12.37	16.96	26.60	4.56	12.43	16.95	26.56
Pa	5.49	9.92	18.35	28.60	5.47	9.92	18.33	28.56
U	5.88	11.55	17.21	30.51	5.87	11.56	17.17	30.47
Np	3.11	13.77	18.61	32.34	3.08	13.79	18.58	32.30
Pu	2.39	13.06	19.98	34.12	2.39	13.05	19.95	34.08
Am	1.97	13.67	21.32	35.86	1.97	13.66	21.29	35.82
Cm	7.48	13.67	16.83	37.56	7.47	13.67	16.80	37.52
Bk	2.67	13.44	18.26	32.86	2.67	13.43	18.24	32.82
Cf	3.05	13.29	19.65	34.61	3.04	13.28	19.62	34.57
Es	3.44	13.11	20.99	36.31	3.44	13.10	20.96	36.27
Fm	3.86	12.91	22.30	37.98	3.86	12.89	22.27	37.94
Md	4.31	12.67	23.59	39.61	4.30	12.66	23.56	39.57
No	5.42	11.77	24.86	41.22	5.42	11.76	24.82	41.18
Lr	3.56	13.04	20.53	42.80	3.55	13.03	20.51	42.75
MAD	0.01	0.00	0.03	0.04				

[a] Results of SAHF Calculations with the DKH2 Hamiltonian.

with the obvious exception of Ac^{3+} that looses a 6p electron from the radon core. The results, collected in Table 5, show negligible differences between the UGBS and SARC values. Specifically, for IE_1 and IE_2 the mean average deviation is close to zero. It is only for the third and fourth ionization energies that the deviations rise slightly, to 0.03 and 0.04 eV, respectively. Importantly, these deviations between SARC and UGBS are consistent for each step in the ionization process and entirely systematic across the whole series. No pathological cases can be identified. We note that the ZORA Hamiltonian produces identical average deviations between SARC and UGBS. Therefore, we conclude that regardless of the scalar relativistic Hamiltonian employed, the SARC basis sets are unlikely to become the accuracy-limiting factor in molecular applications involving changes in actinide oxidation states.

In terms of absolute numerical values, the uncorrelated SAHF ionization energies reported in Table 5 are obviously not to be compared with experiment or high-level calculations. They only serve as a reliable and unambiguous internal consistency check. As mentioned above, accurate prediction of ionization energies requires an adequate treatment of differential electron correlation effects, while spin−orbit coupling must additionally be taken into account especially for the third and fourth ionization processes. DFT within a scalar relativistic framework is arguably not the best-suited approach for this problem, given the compounded shortcomings of the assumed functional form, the single-determinant Kohn−Sham formulation, and the neglect of spin-dependent relativistic corrections. Nevertheless, simply to demonstrate how even an approximate DFT treatment greatly improves the predicted ionization energies, in Table 6 we compare B3LYP/SARC-DKH2 results with high-quality theoretically predicted values[70] as well as with available experimental data on IE_1. The ab initio reference values were obtained from multireference averaged coupled-pair functional (CASSCF/ACPF) small-core pseudopotential (PP) calculations employing large uncontracted valence basis sets, extrapolated to the basis set limit and corrected for spin−orbit interaction and estimated PP-related

Table 6. Comparison of B3LYP/SARC-DKH2 Ionization Energies (eV) with Ab initio Reference Values[70] and Experimental Data

	B3LYP/SARC-DKH2				ACPF/PP				Expt.
	IE_1	IE_2	IE_3	IE_4	IE_1	IE_2	IE_3	IE_4	IE_1
Ac	5.18	11.69	17.63	46.77	5.17	11.60	17.39	44.99	5.17
Th	6.21	11.98	17.91	29.00	6.25	12.11	18.30	28.45	6.31
Pa	5.63	12.16	18.53	31.23	5.81	11.96	17.73	31.24	5.90
U	5.45	11.94	19.30	33.03	6.06	11.63	19.07	33.17	6.19
Np	5.77	11.74	20.45	34.39	5.98	11.35	19.92	34.27	6.27
Pu	5.82	11.85	21.90	35.76	5.71	11.50	21.37	35.43	6.03
Am	5.88	12.02	23.45	37.34	5.71	11.71	22.34	37.26	5.97
Cm	5.60	12.50	20.67	39.23	5.68	12.17	20.36	39.06	5.99
Bk	6.13	12.31	22.33	36.49	5.90	11.96	21.93	36.52	6.20
Cf	6.24	12.45	23.60	38.50	5.96	12.03	22.84	38.12	6.28
Es	6.34	12.58	24.38	40.07	6.07	12.20	23.06	39.52	6.37
Fm	6.45	12.72	25.01	41.18	6.18	12.38	23.66	40.16	6.50
Md	6.54	12.86	26.38	42.10	6.25	12.47	24.69	40.60	6.58
No	6.64	12.99	27.69	43.68	6.33	12.58	26.05	41.96	6.65
Lr	4.56	14.53	21.96	45.28	4.78	14.25	21.52	44.12	–

errors. Thus, they represent one of the currently most reliable sets of theoretical predictions, going beyond what can be expected from the rather rudimentary B3LYP-DKH2 approach.

B3LYP values are in reasonable agreement with the ACPF reference for IE_1 and IE_2, within 0.07 and 0.25 eV on average, respectively. Larger differences are observed for the third and fourth ionization energies, where a distinction can be made between the first and second half of the actinide series: for both IE_3 and IE_4 the highest deviations, often exceeding 1 eV, are witnessed for elements in the second half of the series. In these cases B3LYP systematically overestimates the ionization energy compared to the ACPF reference. With respect to available IE_1 experimental estimates the B3LYP values yield an average deviation of 0.18 eV. In view of the inherent limitations of the present DFT scalar relativistic approach, the above results can be regarded as adequate considering the intended realm of molecular applications; the interested reader is referred to the literature for examples of more rigorous theoretical approaches to the prediction of actinide ionization energies.[20,70−72]

2.4. Basis Set Superposition Errors. A critical factor that impacts on the accuracy of computational studies of molecular complexes is the error introduced by the incompleteness of the atomic basis sets in the valence region. This results in the well-known basis set superposition error (BSSE) and its typical manifestation is the artificial stabilization of a two-fragment system through the mutual compensation of each fragment's incomplete valence space by valence basis functions of the other. The BSSE can be magnified when a heavy and a light atom are adjacent, since the potential for overlap between a relatively big and a relatively small basis set amplifies the effect of basis set imbalance. Boys and Bernardi have proposed the counterpoise correction method (CPC) in order to obtain results that are approximately free of the superposition error,[73] and this is the method we use here to quantify the extent of the BSSE associated with the SARC basis sets. For this purpose we have performed calculations with the DKH2 Hamiltonian and the PBE0 hybrid functional[74,75] on a set of diatomic actinide molecules consisting of one terminal element of the actinide series, Ac or Lr, and one of the light atoms H, O, and F. The DKH2-recontracted versions of the def2-TZVP basis sets were used for the nonactinide elements.[60] Note that the hydrides are particularly sensitive to BSSE since they involve a combination of elements that are at diametrically opposite positions of the periodic table.

Table 7. Bond Lengths r (Å) and Dissociation Energies D_e (eV) of Actinium and Lawrencium Diatomics Computed with the PBE0 Density Functional and the DKH2 Hamiltonian, without and with BSSE Counterpoise Corrections (CPC)

	PBE0/SARC		PBE0/SARC+CPC			
	r	D_e	r	D_e	Δr	ΔD_e
AcH ($^1\Sigma$)	2.128	2.86	2.129	2.85	0.001	−0.01
AcO ($^2\Sigma$)	1.915	7.37	1.915	7.35	0.000	−0.02
AcF ($^1\Sigma$)	2.098	6.99	2.098	6.96	0.000	−0.03
LrH ($^1\Sigma$)	1.976	3.17	1.977	3.17	0.001	0.00
LrO ($^2\Sigma$)	1.853	6.09	1.853	6.06	0.000	−0.03
LrF ($^1\Sigma$)	1.989	7.19	1.990	7.17	0.001	−0.02

The optimized bond lengths (Table 7) display the expected contraction on passing from the lightest to the heaviest actinide. The extent of the contraction is different for each class of compound, being largest for the monohydrides and smallest for the monoxides. This has been pointed out previously for both the lanthanides[76] and the actinides,[77] and results from the fact that bonds with large force constants undergo smaller contractions along the series.[77] It is worth noting that inclusion of spin−orbit effects in addition to scalar relativity has been shown to slightly shorten the predicted bond lengths.[77] For our purposes, the most important conclusion drawn from the comparison of the computed bond lengths for each dimer with and without counterpoise corrections is that the impact of BSSE on bond lengths never exceeds 0.001 Å. Equally small is the BSSE error in predicted dissociation energies, where the uncorrected values are overstabilized by at most 0.03 eV. Thus, these results provide additional confirmation that the incompleteness errors described previously in comparison with the UGBS atomic energies indeed arise from the chemically inert core shells. In conclusion, the results on the diatomic molecules of Table 7 suggest that the SARC valence space is sufficiently extended to ensure minimal BSSE in molecular DFT calculations.

2.5. Uranium Fluorides. The series UF_n (n = 1−6) is quite well characterized experimentally. Especially abundant is experimental data on UF_6, which plays a central role in ^{235}U-enrichment processes by diffusion or centrifugation. Hence, it is not surprising that the uranium fluorides, and to a lesser extent the chlorides, have seen extensive use as reference systems for the evaluation of computational methods.[7,19,26,78−82] Here we test the SARC basis sets on the UF_n series of molecules (Scheme 1) using the ZORA Hamiltonian with the PBE0 functional, in order to make comparisons with experiment and recent theoretical studies. PBE0 has been shown to perform well for a variety of heavy-element systems[61] including the actinide species under consideration.[80] ZORA-recontracted TZVP basis sets have been used for fluorine. All calculations were performed with ORCA using the one-center approximation for ZORA, tight optimization and SCF convergence criteria, increased integration grids (Grid4 in ORCA convention), and taking advantage of the chain-of-spheres (RIJCOSX) algorithm for exact exchange.[83]

Beginning with the heaviest member first, UF_6 is predicted to have an octahedral coordination geometry (O_h point group) with

Scheme 1. Structures of the Uranium Fluorides

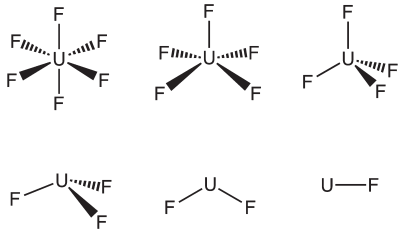

U−F bond lengths of 1.997 Å. In comparison, PBE0 calculations with small-core (60-electron) and large-core (78-electron) effective core potentials for uranium gave U−F bond lengths of 1.993 Å and 2.006 Å, respectively.[26,80] The current PBE0/SARC value is consistent with the two estimates obtained through electron diffraction experiments, 1.999(3) and 1.996(8) Å.[84,85] UF_5 has a doublet ground state with one unpaired electron in the $5f_{xyz}$ orbital of uranium. Its structure is predicted to be C_{4v} symmetric, in agreement with IR spectra obtained in Ar and Ne matrices.[86] The equatorial and axial bond lengths are almost equal, 2.019 and 2.018 Å, respectively, while the uranium atom is axially displaced (0.272 Å) above the plane defined by the four equivalent fluorine atoms, resulting in an obtuse $F_{ax}-U-F_{eq}$ angle of 97.8°. As with UF_6, the SARC bond lengths are ca. 0.004 Å longer than small-core ECP results.[26,80]

When T_d point group symmetry is enforced, the optimized U−F bond length in UF_4 is 2.059 Å, which is identical to the experimentally deduced value by Konings et al.[87] In comparison, PBE0 with small-core ECPs gave a value of 2.053 Å.[80] By removing all symmetry constraints the optimized structure distorts and settles into a C_{2v} symmetric geometry with two pairs of equivalent bonds, 2.054 and 2.060 Å, forming between them angles of 105.9° and 104.7°, respectively. However, the energy gain associated with this distortion is so small (less than 0.4 kcal mol^{-1}) that quantitatively distinguishing between this and other proximate structures[88] for UF_4 would probably require a more fine-grained theoretical approach and explicit consideration of competing Jahn−Teller and spin−orbit effects.[89]

For UF_3 a pyramidal C_{3v} structure is predicted, with U−F bond lengths of 2.073 Å and F−U−F angles of 103.9°, as a result of the uranium atom being 0.862 Å away from the plane defined by the fluorides. UF_2 (quintet ground state) belongs to the C_{2v} point group with bond lengths of 2.067 Å and an F−U−F angle of 109.0°. Finally, the optimized bond length of UF (quartet ground state) is 2.032 Å. The small-core ECP bond lengths for the last three members of the series were reported as 2.069, 2.055, and 2.024 Å, respectively.[80] As with all UF_n species, the ECP bond lengths are consistently shorter than the SARC ones, but the predicted trend is the same with either method, the U−F bond lengths increasing in the order $UF_6 < UF_5 < UF < UF_4 < UF_2 < UF_3$.

Beyond geometries, an interesting metric for our testing purposes are the fluorine bond dissociation energies (BDEs) for the reactions $UF_n \rightarrow UF_{n-1} + F$. Thermochemical studies of uranium fluorides have led to experimental BDEs for the whole series,[90] while the subject has also been the focus of recent theoretical studies.[26,80,82] It is worth reminding that the use of large-core ECPs for BDEs leads to unacceptable errors.[26] In order to ensure that the consistent performance of the presently proposed basis sets extends also to this kind of property, we have computed the successive BDEs of the uranium fluorides at the PBE0/SARC-ZORA level. The BDE of a given species is defined as $BDE(UF_n) = E(UF_{n-1}) + E(F) - E(UF_n)$. Zero-point energy corrections are small and were shown to account for less than 2 kcal mol^{-1} of the total BDE,[26] therefore they are not included in the present calculations. The results are summarized in Table 8, where a comparison is also made with computed values from small-core ECP calculations[80] and all-electron scalar and nuclear-only spin−orbit DKH3 calculations[82] as well as with the experimental values proposed by Hildenbrand and Lau.[90]

Table 8. Comparison Between Calculated PBE0 Bond Dissociation Energies (kcal mol^{-1}) and Experimental Values for the Uranium Fluoride Series

	UF_6	UF_5	UF_4	UF_3	UF_2	UF
SARC-ZORA	70.2	94.1	133.4	143.0	144.4	159.5
60e-ECP[a]	71.4	94.6	137.2	144.7	146.6	155.9
scalar-DKH3[b]	74.5	98.2	140.8	146.5	146.1	164.1
SO−DKH3[b]	70.8	92.5	138.7	146.7	145.2	166.1
expt.[c]	71.0	98.0	147.0	147.9	135.0	154.9

[a] Ref 73. [b] Ref 75. [c] Ref 83.

Table 9. PBE0/SARC-ZORA Vibrational Frequencies of UF_6 (cm^{-1}) Compared with PBE0/ECP Results (Ref 26) and with Experiment (Ref 91)[a]

	ω_1 (a_{1g})	ω_2 (e_g)	ω_3 (t_{1u})	ω_4 (t_{1u})	ω_5 (t_{2g})	ω_6 (t_{2u})	MAD ν /ω
SARC-ZORA	673	536	627	184	201	142	2/3
78e−ECP	644	522	626	191	182	148	11/14
60e−ECP	677	532	631	186	198	140	4/4
expt. (ν)	667	534	626	186	200	143	
expt. (ω)[b]	672	540	634	186	200	143	

[a] Mean absolute deviations (cm^{-1}) are provided with respect to both experimental fundamentals (ν) and estimated harmonic frequencies (ω). [b] Estimated harmonic frequencies.

Inspection of the computed BDEs reveals no significant discrepancy between the different theoretical approaches. The predicted values for most of the molecules agree particularly well among the different methods. Compared to the experimental estimates, UF_4 and UF_2 stand out as the two species for which experiment diverges more obviously from the theoretical predictions. Although all methods are in close agreement for the BDE of UF_2, the experimental estimate is approximately 10 kcal mol^{-1} lower than the theoretical prediction. Exactly the opposite situation is observed for UF_4, for which the experimental estimate is consistently higher than the computed values. Overall, all theoretical methods predict the same order of monotonically increasing BDEs from UF_6 to UF, with a possible exception when passing from UF_3 to UF_2, where a small decrease might be anticipated, arising from the extra stabilization imparted to UF by the pairing of electrons in the uranium 7s orbital.

Finally, it is interesting to see how the present approach performs for the vibrational frequencies of the thoroughly characterized UF_6 molecule. In Table 9 a comparison is made between the current PBE0/SARC-ZORA harmonic vibrational frequencies, PBE0/ECP values previously obtained[26] with either a large-core (78-electron) or a small-core (60-electron) relativistic effective core potential for uranium, and experimental

fundamentals as well as estimated harmonic frequencies by McDowell et al.[91] The PBE0/SARC-ZORA results agree remarkably well with experiment and have the lowest average deviation, 2 cm^{-1} compared to 4 cm^{-1} for the small-core ECP and 11 cm^{-1} for the large-core ECP (3, 14, and 4 cm^{-1}, respectively, in comparison to the projected experimental harmonic frequencies). We consider the advantage of SARC over the small-core ECP too small in absolute terms to be interpreted as a definite improvement, particularly because the average errors of the two approaches are of the same order of magnitude as: (a) the anharmonicity effects, at least in the case of the three higher vibrations, and (b) the experimental uncertainties.[91] With regard to intensities, the intensity ratio I_3/I_4 of the two IR-active vibrations, the ω_3 stretching and the ω_4 bending mode, is predicted to be 19.7 from the PBE0/SARC calculations. This value is in nearly perfect agreement with the experimental ratio of 20.[91] In conclusion, the computed data on vibrational frequencies suggest that the SARC results can be expected to be at least as good as, or slightly better than results obtained with small-core pseudopotentials, and can therefore serve to either cross-validate ECPs for DFT studies or directly improve on their predictions.

3. CONCLUSIONS

Segmented all-electron relativistically contracted (SARC) basis sets are proposed for the 5f elements. These basis sets extend the existing SARC family of basis sets to encompass the whole series of the actinide elements. The basis sets are designed to be of moderate size and polarization, so that they can be used efficiently in routine all-electron DFT calculations employing one of the most popular ZORA or DKH scalar relativistic Hamiltonians. In comparison to results obtained with extended basis sets of more than double their size (UGBS), the SARC basis sets display controlled incompleteness errors that primarily originate from the inner shells. The contraction pattern that is adopted accounts for a minor (ca. 4%) and systematic percentage of the incompleteness error. Comparison of the first four ionization energies of all actinides computed with SARC and UGBS demonstrates near-coincidence for IE_1 and IE_2, while marginal deviations of 0.03 and 0.04 eV are observed for IE_3 and IE_4. Thus, despite the reduction in size, SARC valence properties are still described at a quality close to that of the much larger basis set reference. Investigation of the basis set superposition errors in six actinide diatomic molecules MX (M = Ac, Lr; X = H, O, F) revealed maximum BSSE corrections of 0.001 Å in bond lengths and 0.03 eV in bond dissociation energies. These results confirm that the SARC valence space can be considered balanced and sufficiently saturated for applications based on DFT methods, which do not require extensive polarization to obtain converged results. An illustrative application to uranium fluorides confirms that the SARC basis sets perform well for molecular properties such as geometries, vibrational frequencies and bond dissociation energies. Therefore, we expect the SARC basis sets to be a useful addition to the modern toolbox of computational actinide chemistry.

■ ASSOCIATED CONTENT

Supporting Information. Full listings of the SARC basis sets. This material is available free of charge via the Internet at http://pubs.acs.org.

■ AUTHOR INFORMATION

Corresponding Author

*E-mail: pantazis@thch.uni-bonn.de (D.A.P.).

■ ACKNOWLEDGMENT

We gratefully acknowledge financial support from the Max Planck Society.

■ REFERENCES

(1) Cotton, S. *Lanthanide and Actinide Chemistry*. 2nd ed.; John Wiley & Sons: Chichester, U.K., 2006; p 280.
(2) Kaltsoyannis, N.; Hay, P. J.; Li, J.; Blaudeau, J. P.; Bursten, B. E. Theoretical studies of the electronic structure of compounds of the actinide elements. In *The Chemistry of the Actinide and Transactinide Elements*, 3rd ed.; Morss, L. R., Edelstein, N., Fuger, J., Eds. Springer: Dordrecht, The Netherlands, 2006; pp 1893−2012.
(3) Schreckenbach, G.; Shamov, G. A. *Acc. Chem. Res.* **2009**, *43*, 19–29.
(4) Kaltsoyannis, N. *Chem. Soc. Rev.* **2003**, *32*, 9–16.
(5) Cao, X.; Dolg, M. *Coord. Chem. Rev.* **2006**, *250*, 900–910.
(6) Vallet, V.; Macak, P.; Wahlgren, U.; Grenthe, I. *Theor. Chem. Acc.* **2006**, *115*, 145–160.
(7) Schreckenbach, G.; Hay, P. J.; Martin, R. L. *J. Comput. Chem.* **1999**, *20*, 70–90.
(8) Kirker, I.; Kaltsoyannis, N. *Dalton Trans.* **2011**, *40*, 124–131.
(9) Tassell, M. J.; Kaltsoyannis, N. *Dalton Trans.* **2010**, *39*, 6719–6725.
(10) Tsipis, A. C.; Kefalidis, C. E.; Tsipis, C. A. *J. Am. Chem. Soc.* **2008**, *130*, 9144–9155.
(11) Vetere, V.; Maldivi, P.; Roos, B. O.; Adamo, C. *J. Phys. Chem. A* **2009**, *113*, 14760–14765.
(12) Ingram, K. I. M.; Tassell, M. J.; Gaunt, A. J.; Kaltsoyannis, N. *Inorg. Chem.* **2008**, *47*, 7824–7833.
(13) Hayton, T. W. *Dalton Trans.* **2010**, *39*, 1145–1158.
(14) Dyall, K. G.; Faegri, K. *Introduction to Relativistic Quantum Chemistry*; Oxford University Press: Oxford, 2007; p 544.
(15) de Jong, W. A.; Harrison, R. J.; Nichols, J. A.; Dixon, D. A. *Theor. Chem. Acc.* **2001**, *107*, 22–26.
(16) Dirac, P. A. M. *Proc. R. Soc. London, Ser. A* **1928**, *117*, 610–624.
(17) Ermler, W. C.; Ross, R. B.; Christiansen, P. A. *Int. J. Quantum Chem.* **1991**, *40*, 829–846.
(18) Küchle, W.; Dolg, M.; Stoll, H.; Preuss, H. *J. Chem. Phys.* **1994**, *100*, 7535–7542.
(19) Hay, P. J.; Martin, R. L. *J. Chem. Phys.* **1998**, *109*, 3875–3881.
(20) Cao, X.; Dolg, M.; Stoll, H. *J. Chem. Phys.* **2003**, *118*, 487–496.
(21) Dolg, M.; Cao, X. *J. Phys. Chem. A* **2009**, *113*, 12573–12581.
(22) Koch, W.; Holthausen, M. C. *A Chemist's Guide to Density Functional Theory*. 2nd ed.; Wiley-VCH: Weinheim, Germany, 2001; p 300.
(23) Parr, R. G.; Yang, W. *Density-Functional Theory of Atoms and Molecules*; Oxford University Press: Oxford, 1989; p 352.
(24) Odoh, S. O.; Schreckenbach, G. *J. Phys. Chem. A* **2009**, *114*, 1957–1963.
(25) Iché-Tarrat, N.; Marsden, C. J. *J. Phys. Chem. A* **2008**, *112*, 7632–7642.
(26) Batista, E. R.; Martin, R. L.; Hay, P. J.; Peralta, J. E.; Scuseria, G. E. *J. Chem. Phys.* **2004**, *121*, 2144–2150.
(27) Schreckenbach, G. *Int. J. Quantum Chem.* **2005**, *101*, 372–380.
(28) Fillaux, C.; Berthet, J. C.; Conradson, S. D.; Guilbaud, P.; Guillaumont, D.; Hennig, C.; Moisy, P.; Roques, J.; Simoni, E.; Shuh, D. K.; Tyliszczak, T.; Castro-Rodriguez, I.; Den Auwer, C. *C. R. Chim.* **2007**, *10*, 859–871.
(29) Fillaux, C.; Den Auwer, C.; Guillaumont, D.; Shuh, D. K.; Tyliszczak, T. *J. Alloys Compd.* **2007**, *444*−*445*, 443–446.

(30) Den Auwer, C.; Simoni, E.; Conradson, S.; Madic, C. *Eur. J. Inorg. Chem.* **2003**, *2003*, 3843–3859.
(31) Denecke, M. A. *Coord. Chem. Rev.* **2006**, *250*, 730–754.
(32) Bader, R. F. W. *Atoms in Molecules: A Quantum Theory*; Oxford University Press: Oxford, 1990; p 458.
(33) Becke, A. D.; Edgecombe, K. E. *J. Chem. Phys.* **1990**, *92*, 5397–5403.
(34) Petit, L.; Joubert, L.; Maldivi, P.; Adamo, C. *J. Am. Chem. Soc.* **2006**, *128*, 2190–2191.
(35) Vyboishchikov, S. F.; Sierraalta, A.; Frenking, G. *J. Comput. Chem.* **1997**, *18*, 416–429.
(36) Dyall, K. *Theor. Chem. Acc.* **2007**, *117*, 491–500.
(37) Faegri, K. *Theor. Chem. Acc.* **2001**, *105*, 252–258.
(38) Faegri, K. *Chem. Phys.* **2005**, *311*, 25–34.
(39) Minami, T.; Matsuoka, O. *Theor. Chem. Acc.* **1995**, *90*, 27–39.
(40) Tsuchiya, T.; Abe, M.; Nakajima, T.; Hirao, K. *J. Chem. Phys.* **2001**, *115*, 4463–4472.
(41) Nakajima, T.; Hirao, K. *J. Chem. Phys.* **2002**, *116*, 8270–8275.
(42) Noro, T.; Sekiya, M.; Osanai, Y.; Koga, T.; Matsuyama, H. *J. Comput. Chem.* **2007**, *28*, 2511–2516.
(43) Douglas, M.; Kroll, N. M. *Ann. Phys.* **1974**, *82*, 89–155.
(44) Hess, B. A. *Phys. Rev. A: At., Mol., Opt. Phys.* **1985**, *32*, 756–763.
(45) Hess, B. A. *Phys. Rev. A: At., Mol., Opt. Phys.* **1986**, *33*, 3742–3748.
(46) Jansen, G.; Hess, B. A. *Phys. Rev. A: At., Mol., Opt. Phys.* **1989**, *39*, 6016–6017.
(47) Wolf, A.; Reiher, M.; Hess, B. A. *J. Chem. Phys.* **2002**, *117*, 9215–9226.
(48) van Lenthe, E.; Baerends, E. J.; Snijders, J. G. *J. Chem. Phys.* **1994**, *101*, 9783–9792.
(49) van Lenthe, E.; Snijders, J. G.; Baerends, E. J. *J. Chem. Phys.* **1996**, *105*, 6505–6516.
(50) van Wüllen, C. *J. Chem. Phys.* **1998**, *109*, 392–399.
(51) Laikov, D. N.; Ustynyuk, Y. A. *Russ. Chem. Bull.* **2005**, *54*, 820–826.
(52) Dyall, K. G. *J. Chem. Phys.* **1994**, *100*, 2118–2127.
(53) Laikov, D. N. *Chem. Phys. Lett.* **2005**, *416*, 116–120.
(54) *Amsterdam Density Functional (ADF)*, 2007.01; SCM, Theoretical Chemistry, Vrije Universiteit: Amsterdam, The Netherlands, 2007.
(55) te Velde, G.; Bickelhaupt, F. M.; Baerends, E. J.; Guerra, C. F.; Van Gisbergen, S. J. A.; Snijders, J. G.; Ziegler, T. *J. Comput. Chem.* **2001**, *22*, 931–967.
(56) Roos, B. O.; Lindh, R.; Malmqvist, P.-Å.; Veryazov, V.; Widmark, P.-O. *Chem. Phys. Lett.* **2005**, *409*, 295–299.
(57) Neese, F. *Coord. Chem. Rev.* **2009**, *253*, 526–563.
(58) Aquino, F.; Govind, N.; Autschbach, J. *J. Chem. Theory Comput.* **2010**, *6*, 2669–2686.
(59) Pantazis, D. A.; Neese, F. *J. Chem. Theory Comput.* **2009**, *5*, 2229–2238.
(60) Pantazis, D. A.; Chen, X. Y.; Landis, C. R.; Neese, F. *J. Chem. Theory Comput.* **2008**, *4*, 908–919.
(61) Bühl, M.; Reimann, C.; Pantazis, D. A.; Bredow, T.; Neese, F. *J. Chem. Theory Comput.* **2008**, *4*, 1449–1459.
(62) Neese, F. *ORCA — an ab initio, Density Functional and Semiempirical Program Package*, v. 2.7.0;Universität Bonn: Bonn, Germany, 2009.
(63) Stavrev, K. K.; Zerner, M. C. *Int. J. Quantum Chem.* **1997**, *65*, 877–884.
(64) Zerner, M. C. *Int. J. Quantum Chem.* **1989**, *35*, 567–575.
(65) Jorge, F. E.; de Castro, E. V. R.; da Silva, A. B. F. *J. Comput. Chem.* **1997**, *18*, 1565–1569.
(66) de Castro, E. V. R.; Jorge, F. E. *J. Chem. Phys.* **1998**, *108*, 5225–5229.
(67) Autschbach, J. *ChemPhysChem* **2009**, *10*, 2274–2283.
(68) Malkin, E.; Malkin, I.; Malkina, O. L.; Malkin, V. G.; Kaupp, M. *Phys. Chem. Chem. Phys.* **2006**, *8*, 4079–4085.
(69) Weigend, F.; Ahlrichs, R. *Phys. Chem. Chem. Phys.* **2005**, *7*, 3297–3305.
(70) Cao, X.; Dolg, M. *Mol. Phys.* **2003**, *101*, 961–969.
(71) Liu, W.; Küchle, W.; Dolg, M. *Phys. Rev. A: At., Mol., Opt. Phys.* **1998**, *58*, 1103.
(72) Cao, X.; Dolg, M. *J. Mol. Struct. (THEOCHEM)* **2004**, *673*, 203–209.
(73) Boys, S. F.; Bernardi, F. *Mol. Phys.* **1970**, *19*, 553–566.
(74) Perdew, J. P.; Burke, K.; Ernzerhof, M. *Phys. Rev. Lett.* **1996**, *77*, 3865–3868.
(75) Adamo, C.; Barone, V. *J. Chem. Phys.* **1999**, *110*, 6158–6170.
(76) Wang, S. G.; Schwarz, W. H. E. *J. Phys. Chem.* **1995**, *99*, 11687–11695.
(77) Küchle, W.; Dolg, M.; Stoll, H. *J. Phys. Chem. A* **1997**, *101*, 7128–7133.
(78) Hay, P. J.; Wadt, W. R.; Kahn, L. R.; Raffenetti, R. C.; Phillips, D. H. *J. Chem. Phys.* **1979**, *71*, 1767–1779.
(79) Han, Y. K. *J. Comput. Chem.* **2001**, *22*, 2010–2017.
(80) Batista, E. R.; Martin, R. L.; Hay, P. J. *J. Chem. Phys.* **2004**, *121*, 11104–11111.
(81) Kovács, A.; Konings, R. J. M. *J. Mol. Struct. (THEOCHEM)* **2004**, *684*, 35–42.
(82) Peralta, J. E.; Batista, E. R.; Scuseria, G. E.; Martin, R. L. *J. Chem. Theory Comput.* **2005**, *1*, 612–616.
(83) Neese, F.; Wennmohs, F.; Hansen, A.; Becker, U. *Chem. Phys.* **2009**, *356*, 98–109.
(84) Seip, H. M. *Acta Chem. Scand.* **1965**, *19*, 1955–1968.
(85) Kimura, M.; Schomaker, V.; Smith, D. W.; Weinstock, B. *J. Chem. Phys.* **1968**, *48*, 4001–4012.
(86) Jones, L. H.; Ekberg, S. *J. Chem. Phys.* **1977**, *67*, 2591–2595.
(87) Konings, R. J. M.; Booij, A. S.; Kovács, A.; Girichev, G. V.; Giricheva, N. I.; Krasnova, O. G. *J. Mol. Struct.* **1996**, *378*, 121–131.
(88) Zhang, Y.; Li, Y.; Cao, Y. *J. Mol. Struct. (THEOCHEM)* **2008**, *864*, 85–88.
(89) David, J.; Fuentealba, P.; Restrepo, A. *Chem. Phys. Lett.* **2008**, *457*, 42–44.
(90) Hildenbrand, D. L.; Lau, K. H. *J. Chem. Phys.* **1991**, *94*, 1420–1425.
(91) McDowell, R. S.; Asprey, L. B.; Paine, R. T. *J. Chem. Phys.* **1974**, *61*, 3571–3580.